Experimental and numerical investigations towards the lateral torsional buckling of cellular steel beams

Nicolas Boissonnade, Joanna Nseir, Hugues Somja

▶ **To cite this version:**

Nicolas Boissonnade, Joanna Nseir, Hugues Somja. Experimental and numerical investigations towards the lateral torsional buckling of cellular steel beams. Thin-Walled Structures, 2024, 195, pp.111388. 10.1016/j.tws.2023.111388 . hal-04467377

HAL Id: hal-04467377

https://univ-rennes.hal.science/hal-04467377

Submitted on 11 Apr 2024

HAL is a multi-disciplinary open access archive for the deposit and dissemination of scientific research documents, whether they are published or not. The documents may come from teaching and research institutions in France or abroad, or from public or private research centers.

L'archive ouverte pluridisciplinaire **HAL**, est destinée au dépôt et à la diffusion de documents scientifiques de niveau recherche, publiés ou non, émanant des établissements d'enseignement et de recherche français ou étrangers, des laboratoires publics ou privés.

Distributed under a Creative Commons Attribution - NonCommercial 4.0 International License

Journal Pre-proof

Experimental and numerical investigations towards the lateral torsional buckling of cellular steel beams

Nicolas Boissonnade, Joanna Nseir and Hugues Somja.

Nicolas Boissonnade, Professor, Civil Engineering Department, Laval University, Québec Canada, Nicolas.boissonnade@gci.ulaval.ca Joanna Nseir, Professor, Civil Engineering Department, University of Applied Sciences of Western Switzerland, Fribourg, Switzerland, joanna.nseir@hefr.ch Hugues Somja, Professor, Institut National des Sciences Appliquées, Rennes, France, Hugues.Somja@insa-rennes.fr Yours, N. Boissonnade.

HIGHLIGHTS

- A series of 3 full-scale bending tests on cellular and Angelina girders is reported;
- 4-pt bending arrangements of beam from 7.5 *m* to 11 *m* span were chosen so as to maximize the occurrence of lateral torsional buckling;
- Careful measurements on material properties (tensile tests) and geometrical imperfections are reported;
- Besides, dedicated non-linear shell F.E. models were developed and validated against the experimental data;
- As excellent agreement between experimental and numerical sources is evidenced, the numerical models are found fit to be used in extensive numerical parametric studies aimed at characterizing in detail the structural response of cellular beams.

Journal Pre-proof

Journal Pre-proof

Abstract

This paper deals with the response of so-called "cellular members" against lateral torsional buckling. These beams comprising regularly-spaced circular web openings are especially used for their high resistance-to-weight ratio, the possibility to integrate service pipes within their height, and for aesthetics. Such profiles usually exhibit a complex behaviour and many potential failure modes, including interactional local/global instability modes. Regarding global instability, the members are usually designed by means of approximate design rules, which often lead to an unduly conservative solution, with beams sometimes showing up to 150% resistance reserves.

The present research works aim at improving this situation, through the development of adequate design formulae. In this respect, the present paper reports on investigations led towards improved solutions for cellular members at the experimental and numerical levels. This first paper focuses on experimental activities and on the development and validation of dedicated shell F.E. models. The results of three bending tests on members spanning from 7.5 *m* to 11 *m* are reported. Cross-sectional dimensions, material properties and accurate initial geometrical imperfections were measured for each specimen and further introduced in the corresponding F.E. models, which are shown to provide predictions in close agreement with the experimental results. The companion paper [1] further makes use of the F.E. models within extensive parametric studies and proposes a new set of design rules that could be proposed for integration in Eurocode 3.

Journal Pre-proof

1. Introduction

The present paper deals with the resistance and stability of so-called "cellular" members (Fig. 1); in particular, attention is paid to their behaviour against Lateral Torsional Buckling (L.T.B.). Cellular members consist of manufactured girders obtained from usual hot-rolled profiles, in such

a way that regularly spaced openings are present within the web height. Typically, castellated (i.e., with hexagonal openings) and cellular (i.e., with circular openings) members are manufactured through the following process:

- In a first step, flame-cutting of the web of a parent H or I rolled member along a specific pattern is performed. Usually, this operation is processed in parallel with multiple members in order to optimize production costs[1]. Different cutting patterns result in different sizes and positions of the openings, for a given parent section (Fig. 2);
- Then, in a second step, the obtained upper and lower tees are separated from each other, translated in the longitudinal direction and welded tip-to-tip together, so that the openings get their final shape (Fig. 2).

Journal Pre-proof

[1] This operation may be repeated twice for cellular members depending on the cutting pattern.

Fig. 1: Castellated (upper) and cellular (bottom) steel members used in frame girders.

Journal Pre-proof

Fig. 2: Fabrication process: principle, flame-cutting and welding of webs' tees.

Accordingly, the final height of the girder is greatly increased, resulting in (i) a higher resistance – thus improving U.L.S. limit states – and (ii) a much greater second moment of area, benefiting to S.L.S. limit states. Nearly all doubly-symmetric structural rolled shapes usually available can be considered for being manufactured into cellular beams, and mixed solutions involving different parent sections and dimensions of the tees to get a wide variety of sections may be used in practice as well. Also, the presence of the openings allows the passage of service pipes through the web, reducing in a considerable extent the total depth of the whole. Moreover, they can be used out of aesthetic considerations due to their light appearance.

Journal Pre-proof

These girders mainly meet their practical and economical relevance for rather long beams, spanning from 12 *m* to 25 *m*; usually, for such lengths, the extra costs resulting from the additional cutting and welding operations are more than compensated by the increase in strength and stiffness and by depth savings. Typically, multi-storey "open-space" office buildings, long-span parking areas, composite floors or medium span portal frames can benefit from these specificities.

Cellular members are mostly used as beam members, i.e., resisting primarily to shear and bending forces. Consequently, the resistance to lateral torsional buckling is crucial for such girders, owing to (i) high height-to-width h / b ratios, (ii) long spans and (iii) lack of lateral bracing, especially during erection phases. Indeed, it is frequent that after welding, cellular beams exhibit 50% or more height than the base hot-rolled profile, leading to an exacerbated sensitivity to lateral torsional buckling.

To date, the practical design of such girders against lateral torsional buckling has been either significantly overestimated or based on rather rough and oversimplified mechanical models, usually disregarding the beneficial influences of the flange in tension, actual torsional stiffness and presence of material between holes (remaining parts of web). In the early 80's, Nethercot and Kerdal [2, 3] conducted a series of experimental tests on castellated beams in bending, dedicated to the identification of specific failure modes. Years later, a European project entitled "Lateral Torsional Buckling in Steel & Composite Beams" [4] was partly devoted to cellular and castellated beams; however, this research project did not investigate the specific L.T.B. behaviour, providing a few tests results and no dedicated design proposal. Additional information may be found in Radic [5], El-Sawy [6] and Sweedan [7], where proposals for the determination of the critical bending moment M_{cr} in cellular and castellated beams are given; several topics

Journal Pre-proof

relative to various other aspects of the behaviour of castellated beams (e.g., distortion) are also treated in Zirakian [8], Lakusic [9], and Ellobody [10]. Many other investigations related to instabilities of cellular or castellated beams may also be found in the literature, such as on flexural buckling behaviour [11] – [13], composite cellular beams [14] – [16]) beam-column behaviour [17] – [19], shear strength of local web-post buckling [20], [21], L.T.B. resistance under fire [22], etc. In 2004, another European project [23] was conducted, however more dedicated to isolated openings, thus not relevant for the present investigations. One may also refer to experimental, numerical and analytical investigations performed on composite cellular and Angelina beams [14] – [16], in which the specific lateral torsional buckling behaviour was however not addressed.

The production process was also shown to have an influence on the residual stresses distribution and a detrimental effect on the resistance to lateral torsional buckling, in increasing the compressive residual stresses at the flanges' tips ([24], [25]). Accordingly, Sonck suggested the use of different buckling curves for cellular or castellated columns and beams to account for the influence of specific residual stresses in these girders. A so-called "2T approach" is presented, involving the remaining material in a section at the centre of an opening – only upper and lower Tees are contributing to the resistance in such a section. The approach is based on Eurocode 3 guidelines to L.T.B. and is limited to constant bending moments; it remains however relatively straightforward to extend to other linear bending moment distributions.

Panedpojaman et al. [26] investigated the influence of shear on the L.T.B. resistance, where important interactions with cross-section capacity characterizing inelastic L.T.B. as well as the influence of specific Virendeel effects were studied. A Eurocode 3-type design approach was proposed, through curve-fitted correction factors accounting for the presence or not of shear

loads. Feirreira et al. [27] investigated the impact of various residual stresses distributions on the L.T.B. resistance and analysed the performance of European and Australian design recommendations as well as other authors proposals. This resulted in a series of design recommendations with respect to L.T.B., Vireendel mechanism and web pot buckling for stocky cellular beams. Rather recently, other authors have also relied on artificial neural networks or similar approaches ([28]) – [31]) to propose numerically or tool-based design approaches to the L.T.B. resistance of cellular beams.

Yet, it may be argued that no fully satisfactory design solutions for the lateral torsional buckling resistance have been reached so far, so that the present set of companion papers reports on investigations led towards improved solutions for the lateral torsional buckling resistance of cellular members, both at the experimental, numerical and design level. The intention is here to characterize the lateral torsional buckling response of such girders, and to propose a practical design approach that better accounts for all aspects previously cited.

The following classical research strategy was adopted:

- Perform a reduced number of experimental tests on cellular and Angelina[2] girders in order to provide reference experimental results;
- Develop F.E. models and validate their adequacy with respect to the experimental results;
- Use the numerical tools to build a database of reference results through extensive parametric studies;
- Investigate various mechanical models able to provide more accurate and economic design formulae, the latter being validated through the F.E. reference results.

[2] So-called “Angelina girders” are built according to the same industrial process but offer mouth-shaped regular openings.

This first paper focuses on experimental activities and on the development of suitable F.E. models, while the companion paper describes numerical and design approach developments. Next Section 2 summarizes preliminary experimental results and data, such as material tests and the measurement of geometrical imperfections; Lateral Torsional Buckling test results are detailed in Section 3. The development and assessment of F.E. models vs. test results are detailed in Section 4, and a fairly good agreement is evidenced between both sources, indicating the potential for the F.E. models to lead to safe and reliable numerical results; the models have been further used in extensive parametric studies, as described in the second paper [1].

2. Preliminary measurements of test specimens

2.1 Material tests

The main bending tests consisted in so-called "4-point" bending tests on two cellular beams (parent sections: HEA 340 and IPE 330, steel grades S355) and on an Angelina beam (parent section: IPE 330, steel grade S235). The base sections were chosen so as to represent common base profiles to be manufactured into cellular or Angelina beams, and their size adjusted to carrying capacities in line with the available testing equipment.

The stress-strain behaviour of the specimens' material was characterized through tensile tests that followed state-of-the art specimen preparation and loading protocols. For each section, two necked coupons were cut from the flanges and web faces. All coupons were extracted in the longitudinal direction of the girders. Engineering stress-strain diagrams (Fig. 3) were built on the basis of the applied force and the measured central cross-section dimensions of each coupon, as well as from accurate extensometer elongation measurements leading to strains; Table 1 reports on the accordingly-measured material properties. The loading protocol (Fig. 3a) included a so-called "descending branch" at 1% strain followed by consecutive strain increments up to

fracture – intention was here to record more data for improved estimates of the Young's modulus, based on multiple values, see Table 1. The obtained σ-ε constitutive laws have also been further introduced in the F.E. models, through multi-linear relationships appropriately representing the average experimental measured data (i.e., linear representations of linear elastic part, plastic plateau, strain hardening zone and necking zone, cf. Section 4); use of linear regression analysis has been made to determine the various parameters needed, see Table 1. Coupons extracted from the Angelina girder had a nominal yield stress of 235 *MPa*, and the tensile test results showed a 20% higher average yield stress. For the HEA 340 with a nominal yield stress of 355 *MPa*, results showed an increase of 35% in yield stress. The IPE 330 exhibited only a 5% increase in yield stress compared to its nominal value of 355 *MPa*.

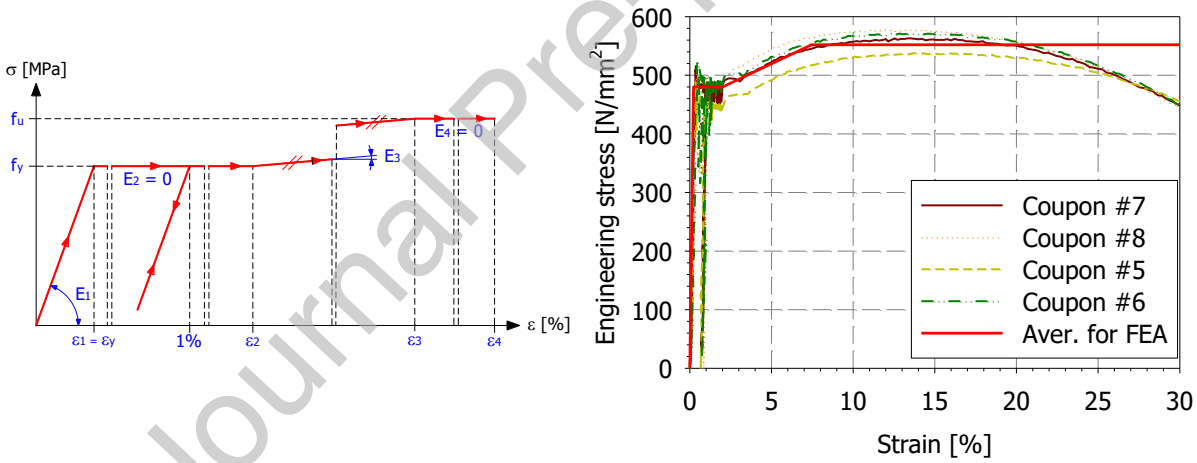

Fig. 3: a) Typical loading protocol for coupon tests – b) Results for "HEA 340 parent section" coupons samples.

Journal Pre-proof

Table 1: Results of the coupon tests.

Coupon # (specimen)	1st slope			2nd slope		3rd slope		4th slope
	f_y [N/mm^2]	ε_1 [%]	E_1[3] [GPa]	ε_2 [%]	f_u [N/mm^2]	ε_3 [%]	E_3 [N/mm^2]	ε_4 [%]
1 (Angelina)	285	0.17	–	1.98	407	6.93	2465	30
2 (Angelina)	283	0.19	–	1.98	393	6.98	2200	30
3 (Angelina)	284	0.18	–	2.00	393	6.99	2184	30
4 (Angelina)	290	0.20	–	2.00	407	7.03	2328	30
Average	*286*	*0.18*	–	*1.99*	*400*	*6.98*	*2294*	*30*
5 (HEA 340)	480	0.20	230.0	2.00	522	7.85	1060	30
6 (HEA 340)	488	0.25	195.2	2.00	565	7.98	1288	30
7 (HEA 340)	482	0.22	219.1	2.00	556	8.01	1231	30
8 (HEA 340)	490	0.24	204.2	2.00	564	6.00	1850	30
Average	*480*	*0.23*	*212.1*	*2.00*	*552*	*7.46*	*1357*	*30*
9 (IPE 330)	373	0.21	–	2.00	481	5.03	3564	30
10 (IPE 330)	372	0.22	–	2.00	480	5.10	3484	25
Average	*373*	*0.22*	–	*2.00*	*481*	*5.07*	*3524*	*28*

2.2 Actual dimensions and geometrical imperfections

Actual geometrical dimensions were measured prior to testing; Table 2 summarizes the recorded data (see also Fig. 4 for notations), where the values reported correspond to averages from measurements taken at various sections along the member. Table 2 also reports on characteristic lengths of the 4-point loading arrangement (see Section 3).

Table 2: Average measured dimensions of tested specimens and lengths.

Specimen	H^* [mm]	B^* [mm]	t_f^* [mm]	t_w^* [mm]	s [mm]	a_0 [mm]	*Number of openings* [–]	*Total span length* [mm]	*Length middle segment* [mm]
Angelina	518.2	160.5	11.9	8.1	1100	380	6	11 000	6 600
HEA 340	468.9	297.4	16.03	10.28	515	345	10	7 500	5 300
IPE 330	446.2	161.5	10.75	7.75	395	345	17	11 000	7 110

[*] H stands for the final height of the section, B the width of the section, t_f and t_w the thickness of flanges and web, respectively.

[3] E_1 Young's Modulus could not be properly measured from Angelina and IPE 330 coupons; a conventional 210 GPa value was adopted in the finite element simulations.

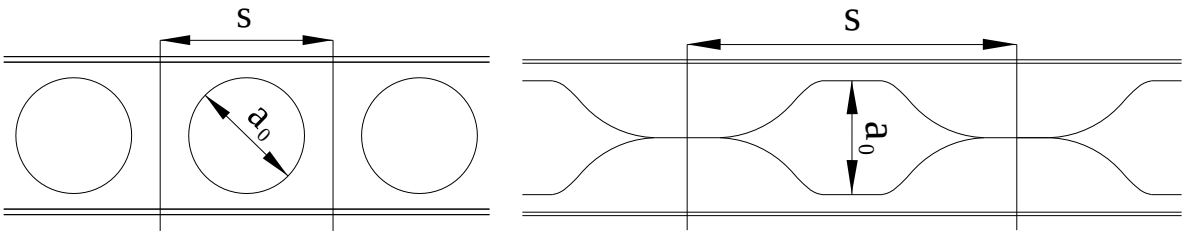

Fig. 4: Geometrical description of tested beams – a) Cellular type – b) Angelina type.

Initial geometrical imperfections were carefully measured through the combination of three improved topometric techniques able to provide a three-dimensional representation of a specimen, providing an overall level of reliability estimated to be around ±0.3 *mm*, which is a remarkable accuracy given the overall dimensions and lengths of the beam specimens (up to 11 000 *mm*, cf. [32]).

First, a "global scanning" of the steel girder was achieved by means of a dedicated theodolite capable of capturing more than 100 000 target points on the member, enabling "clouds of targets" to be established with an accuracy of ±3 *mm* (see Fig. 5). This global scanning was intended at being gradually refined by means of the two complementary procedures described hereafter.

Fig. 5: Global scan of a girder.

The second technique consisted in measuring accurate 3D representations of the flanges' edge lines. This could be done through a purposely-developed optical system, which was able to

measure accurately (±0.2 *mm* accuracy) the position of a "light source" – here, a L.E.D. – placed upon the flange's edge, over a longitudinally-moving trolley (see Fig. 6). For each of the four edges lines, the trolley was displaced – and its position measured – every 5 *cm*, providing an accurate measurement of the edges' lines.

Fig. 6: Measurement of flanges' edges – a) Trolley and L.E.D. light – b) Optical measurement device.

As a third technique, refined scans of some key local areas on the member (200 x 100 *mm*) were made, with an accuracy of ±0.2 *mm*. Both external and internal surfaces of the web have been measured, and, after numerical treatment, an average surface was kept for introduction in the F.E. models (Fig. 7).

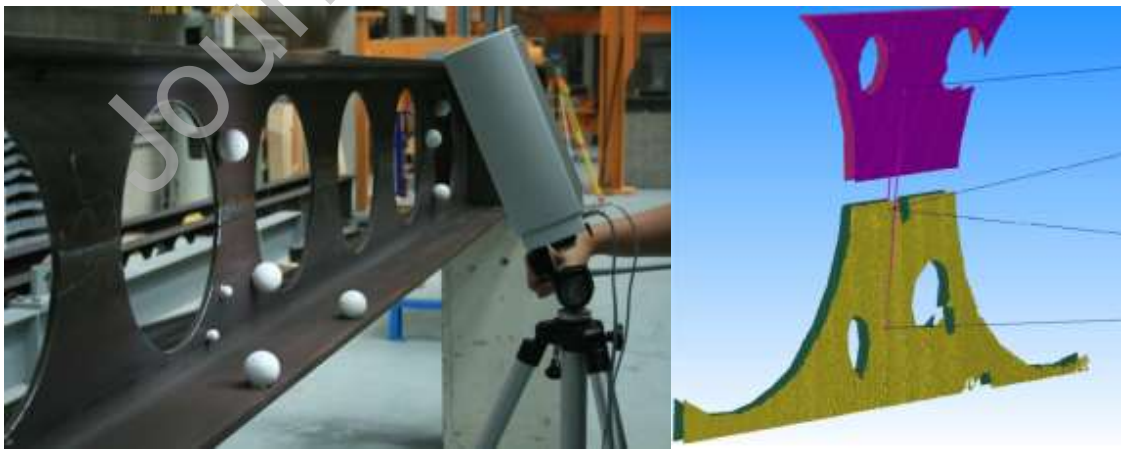

Fig. 7: a) Local scanning of web imperfections – b) Local geometry after numerical treatment.

Journal Pre-proof

All this information was used to provide accurate definitions of imperfect geometries of the F.E. meshes, through sophisticated and rigorous treatments of the measurements, along with interpolation techniques using data from all three sources. Place is missing here to provide the corresponding detailed calculation procedures, but the main steps mainly consisted in (i) getting a (large) cloud of data points from all 3 sources of measurements followed by (ii) topometric treatments to "downsize" this cloud into the F.E. meshes. Accordingly, the nodes of the numerical models accurately accounted for the measured imperfections, through "imperfect" sets of coordinates. Fig. 8 illustrates with magnified views examples of imperfect meshes which were later introduced in the numerical models.

Journal Pre-proof

Fig. 8: Initial geometrical imperfection in web and flanges (magnified 20 times, base profile: HEA 340).

3. Lateral torsional buckling tests

3.1 Experimental setup

Three full-scale bending tests were performed in the Structural Engineering laboratory of the University of Applied Sciences of Western Switzerland – Fribourg, on members spanning from 7.5 *m* to 11.0 *m* (Fig. 9 and Fig. 10). They consisted in so-called "4-point bending" tests on two cellular members (one based on an IPE section and the second based on a HEA structural shape) and on an Angelina girder (Fig. 10). The test arrangement and girders were designed to reach failure in an L.T.B. mode, with different member slenderness. Accordingly, point loads were applied as close as possible to the end supports, in order to maximize the span of the segment acted by constant bending moment. The adjacent segments' openings in the web were filled prior to testing in order to avoid any unintended failure in these regions. Also, vertical stiffeners were welded at the end sections of each girder and at the points of load application.

Journal Pre-proof

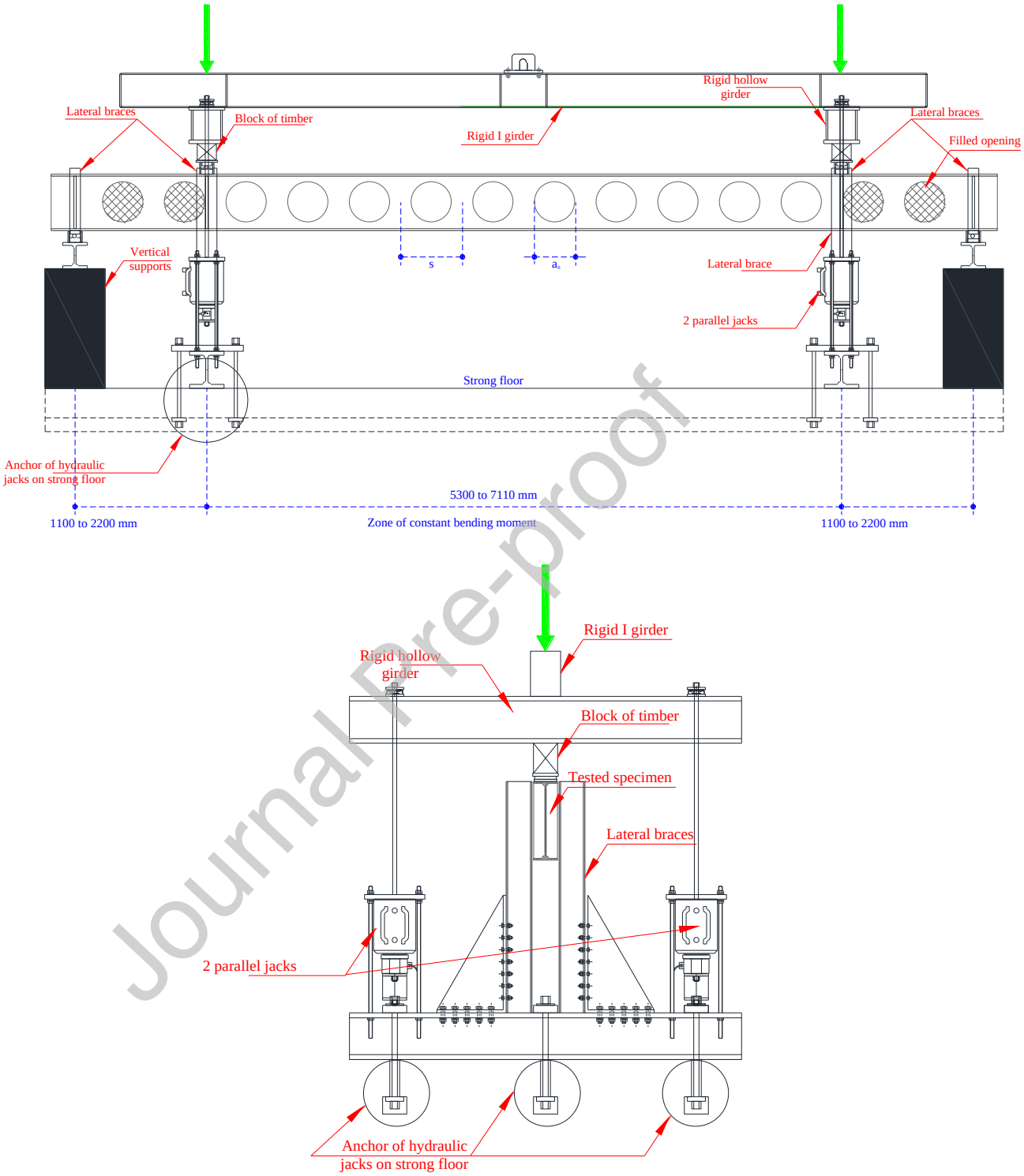

Fig. 9: Test setup (longitudinal and transversal views).

Journal Pre-proof

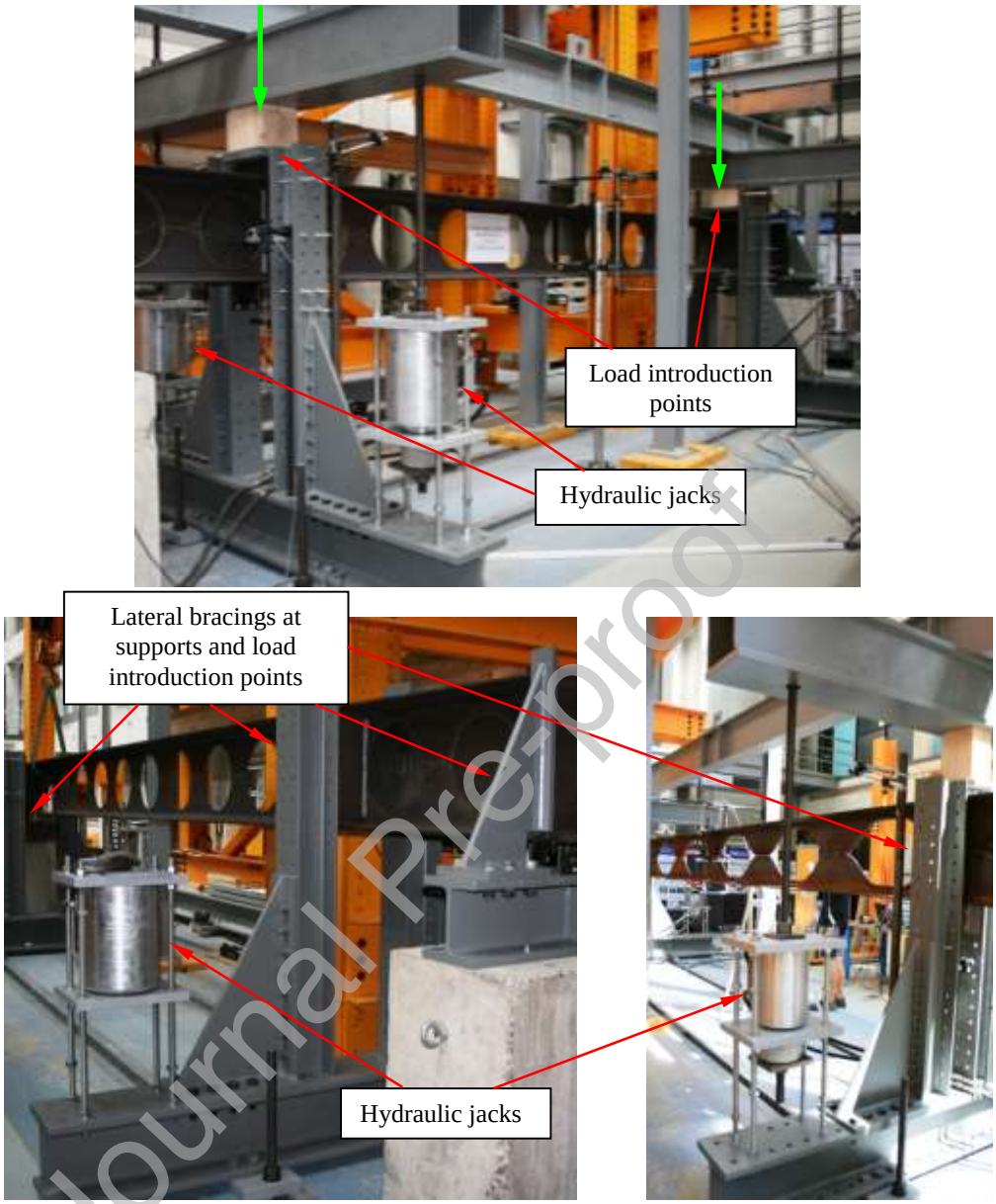

Fig. 10: a) General test setup (4-point bending tests) – b) Supports.

The support arrangement was intended at offering vertical, lateral and torsional twist restraints as schematically represented on Figs. 9 to 11. The usual reference situation of a constant bending moment and fork conditions could not be strictly fulfilled for the middle part of the beam, since the end segments provided flexural (minor-axis) and warping restraints. Moreover, the lateral supporting system may not be seen as providing neither an infinite lateral stiffness nor a strictly punctual lateral support. Nevertheless, lateral displacements at the top and bottom flanges at the

braced sections were monitored during the tests and were shown to be negligible. Accordingly, horizontal fixity of the flanges in these sections could reasonably be assumed; this was carefully taken into account in the F.E. models. Lastly, both the intermediate and end supports could be shown to provide a negligible warping stiffness.

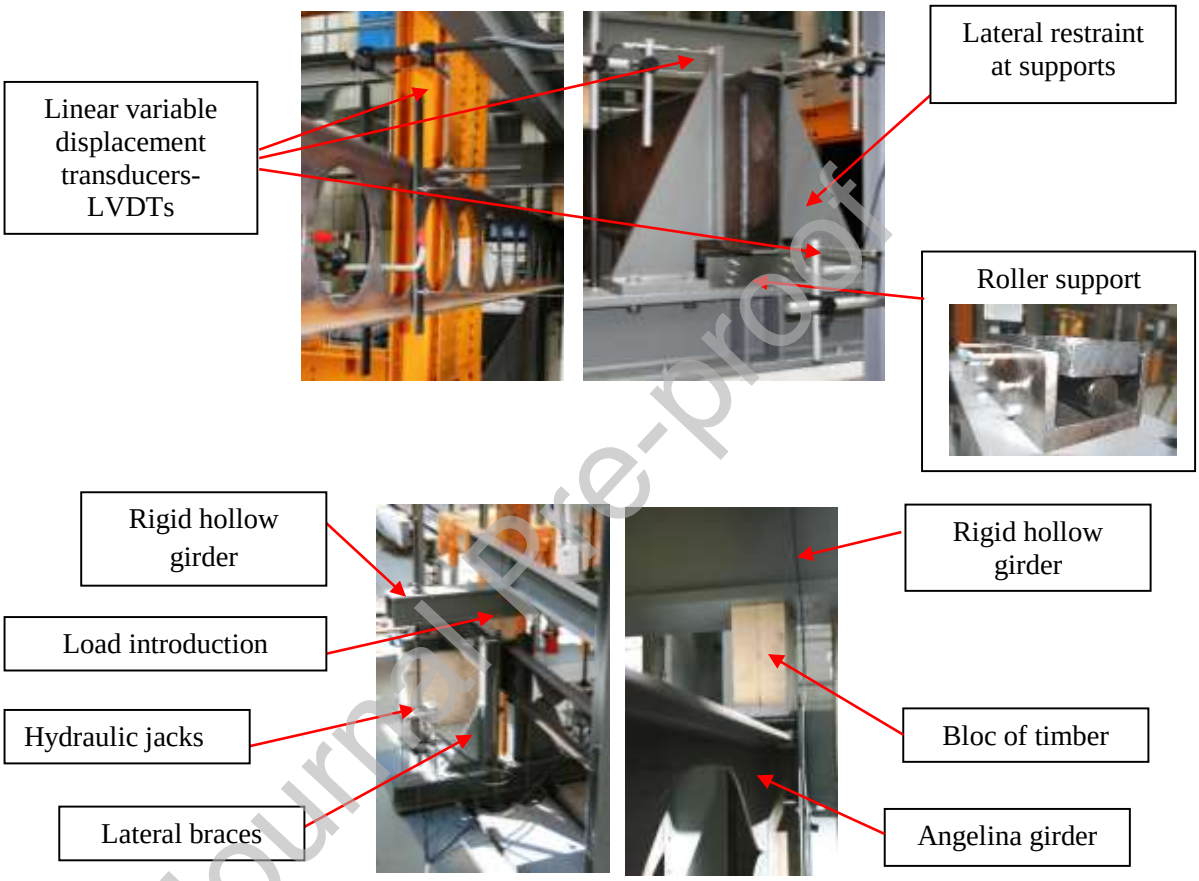

Fig. 11: Load introduction and support condition details.

Loading was applied through the use of four hydraulic jacks – two jacks for each point load – pulling downwards and anchored on the strong floor. Each set of jacks was acting simultaneously and was connected to a rigid hollow girder which, in turn, was placed upon the beam's top flange, applying the vertical point load. In order to let sufficient vertical displacement freedom to the rigid hollow girder, it was relying on a (rigid) bloc of timber whose width was slightly smaller than the flange's width, allowing vertical movement of the point of load

application in between the horizontal braces. Vertical displacements at loading points were measured directly on top of the girder's flange, i.e., free from any influence of this loading system.

In addition to the live control of the applied load, multiple displacements were measured continuously during each test, by means of a combination of 22 L.V.D.T.s. Fig. 11 gives an overview of the positions and nature of the instrumentation used for the end and middle cross-sections. As a specific point, the mid-span cross-section was instrumented with a combination of four L.V.D.T.s, in order to capture information (i) on the vertical displacement of the cross-section, (ii) on the lateral displacement and (iii) on the torsional twist.

3.2 Tests results

All test specimens exhibited a typical lateral torsional buckling failure with the middle span sections experiencing simultaneous vertical and lateral deflections, combined with torsional twist. In the post-peak regime, the sections eventually reached a buckled compression flange, usually far beyond the peak load, where the stresses became localized in the critical section (see Fig. 12). Table 3 summarizes the measured loads and displacements recorded at peak load.

Journal Pre-proof

Fig. 12: Deformed configuration & torsional twist at peak load and residual deformation after unloading (HEA 340 specimen).

Table 3: Results of experimental tests.

Specimen	P_{max} $[kN]$	M_{max} $[kNm]$	$\Delta_{vert.\ max}$ $[mm]$	$\Delta_{lat.\ max}$ $[mm]$	ψ_{max}[1] $[rad]$
HEA 340	1977	1087.4	75.1	15.3[2]	0.035
IPE 330	176.9	172.0	62.3	24.5	0.075
Angelina	235.1	258.6	59.4	6.35	0.015

1. ψ_{max} stands for the measured torsional twist at peak load, and P_{max} represents the total vertical load applied on the member.
2: measurement devices had to be removed from specimen slightly before reaching peak load.

Fig. 13 to Fig. 16 as well as Fig. 17 reflect the behaviour observed during the tests. The response of specimen with HEA 340 parent section was typically “inelastic L.T.B.”. The beam exhibited nearly elastic linear response until peak, with lateral displacement (Fig. 13b) and noticeable torsional twist (Fig. 16a) rapidly increasing beyond applying about 1800 *kN*; the beam’s response is indeed seen to be affected by a quite important drop in stiffness after the loading reached 1800 *kN*. Residual stresses – especially compressive residual stresses at the flange’s tips, cf. [19] – are obviously responsible for this stiffness degradation and the subsequent lateral drift and torsional twist faster increases. The particular and sudden increase in lateral displacement when approaching the maximum load is also noticeable, see Fig. 13b.

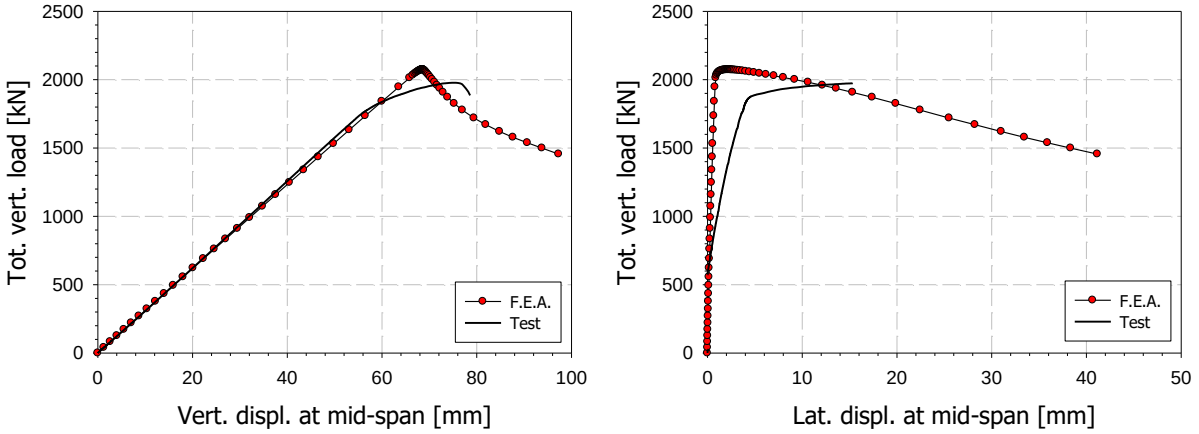

Fig. 13: Load-displacement behaviour – Base profile: HEA 340.

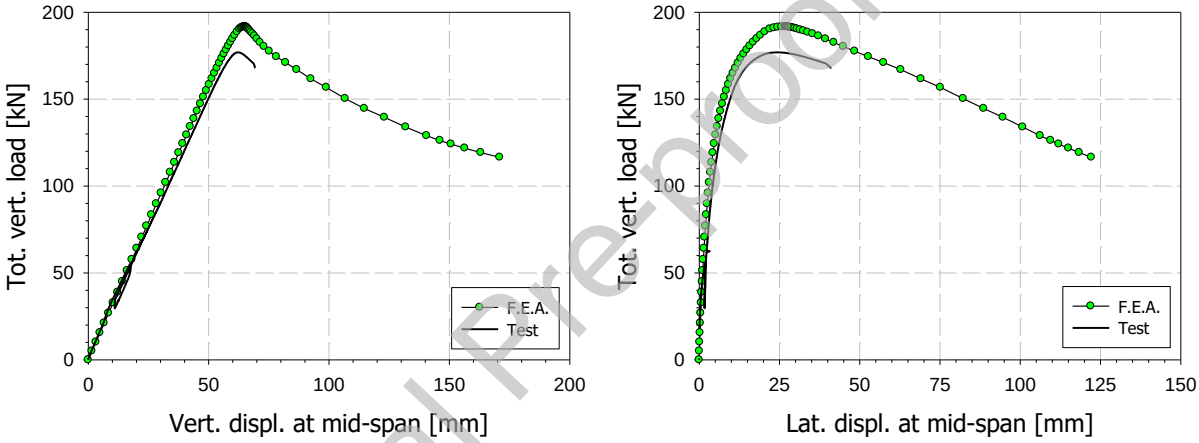

Fig. 14: Load-displacement behaviour – Base profile: IPE 330.

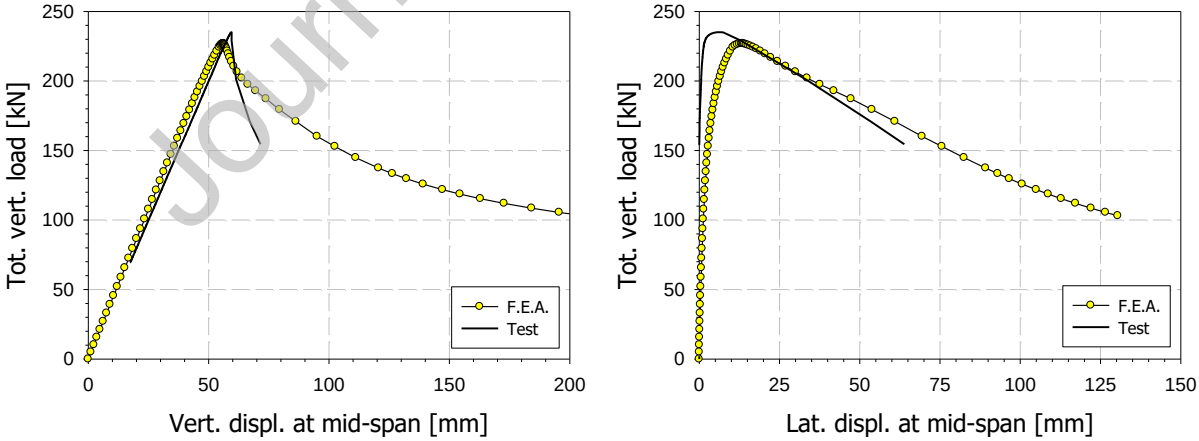

Fig. 15: Load-displacement behaviour – Angelina girder.

Journal Pre-proof

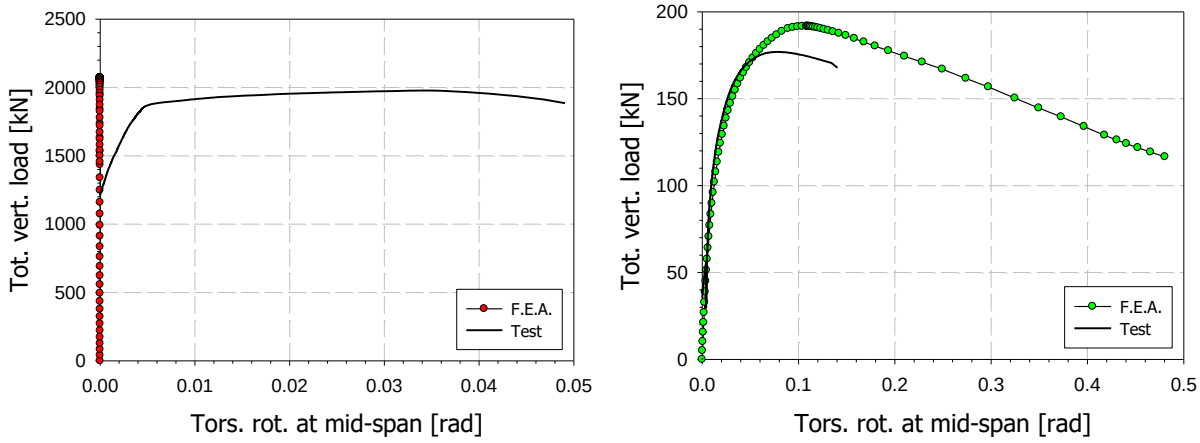

Fig. 16: Torsional response of girders – a) HEA 340 base profile – b) IPE 330 base profile.

In contrast, the other two tests on an Angelina girder and on a cellular beam from parent section IPE 330 were similarly of "elastic L.T.B." type, characterized by sharp decreases in resistance immediately after the elastic part, at load levels quite below the plastic section capacity. Both longer spans and slender parent and final sections are clearly responsible for these slenderer responses.

Table 4: Key mechanical characteristics of the tested girders.

Specimen	$M_{cr,actual}$ [kNm]	$M_{pl,actual}$ [kNm]	λ_{LT} [–]	χ_{LT} [–]	*Diff. to curve a* [%]	$M_{pl,actual,full}$ [kNm]	λ_{LT} [–]	χ_{LT} [–]	*Diff. to curve a* [%]
HEA 340	3658.7	1188.7	0.57	0.91	+1	1335.5	0.60	0.81	-9
IPE 330	220.7	448.7	1.43	0.38	-3	559.6	1.59	0.31	-8
Angelina	302.0	353.8	1.08	0.73	+23	437.5	1.20	0.59	+12

Table 4 and Fig. 17 further allow characterizing how L.T.B.-prone the girders were, by means of L.T.B. reduction factor χ_{LT} – relative L.T.B. slenderness λ_{LT} pairs, where λ_{LT} and χ_{LT} are defined as follows:

$$\overline{\lambda}_{LT} = \sqrt{\frac{M_{pl}}{M_{cr}}} \quad and \quad \chi_{LT} = \frac{M_{\max,test}}{M_{pl}} \tag{1}$$

In Eq. (1), M_{pl} is relative to the actual plastic bending moment of the *weakest* cross-section (i.e., for a section at the middle of an opening), as recommended by various design approaches ([11], [14] and [23]). Exceptions are for $M_{pl,actual,full}$ values in the right part of Table 4 and for square dots in Fig. 17 which relate to *maximum* plastic bending capacities at sections with plain webs (no holes). M_{cr} values were computed numerically from the shell models detailed in the next section, and therefore account for "true" loading and support arrangements; in particular, M_{cr} values take due account of flexural and warping restraints brought to the middle span by the edge segments.

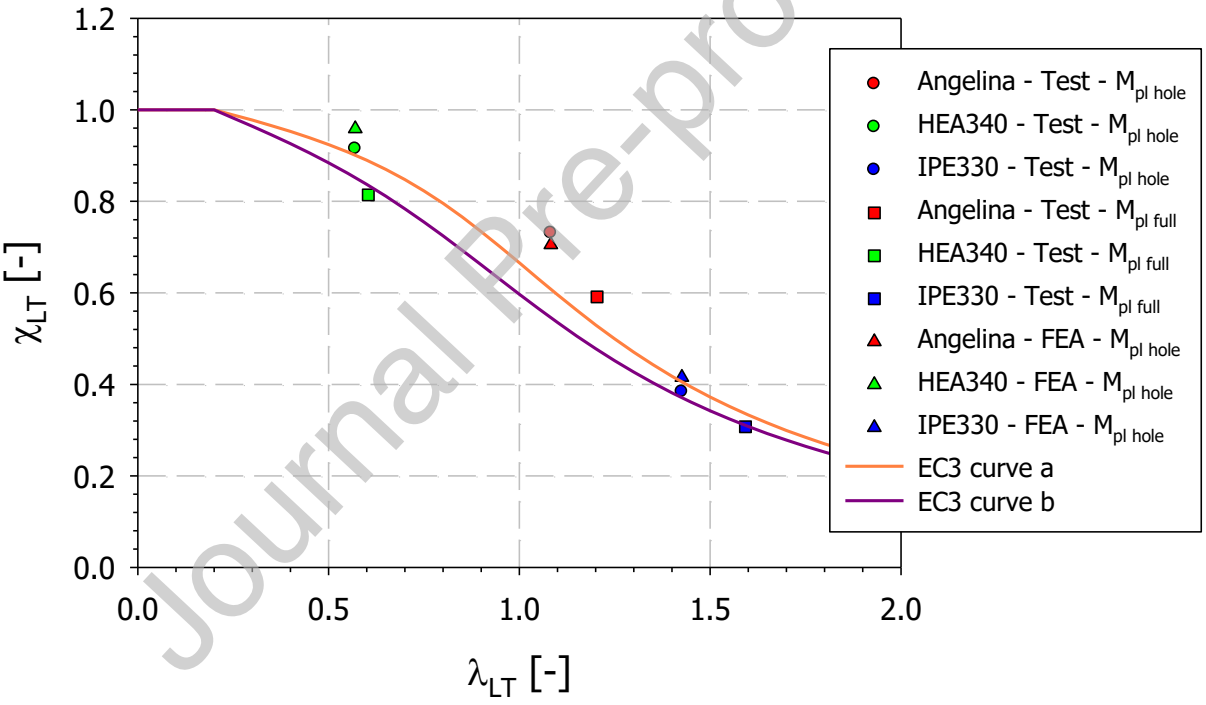

Fig. 17: Test & F.E.A. results compared with Eurocode 3 buckling curves.

Fig. 17 and Table 4 confirm the observed sensitivities to L.T.B. for the HEA 340 parent section test and the other two tests: inelastic L.T.B. response with values of χ_{LT} calculated from

experimental peak loads are close to unity for the former, intermediate to quite low for the other two tests. Fig. 17 also further shows that:

(i) Substitution of $M_{pl\,full}$ instead of $M_{pl\,hole}$ has a significant impact on the resistance prediction at low slenderness for the HEA 340 parent section specimen: χ_{LT} indeed significantly drops while λ_{LT} is only slightly increased;

(ii) Use of $M_{pl\,hole}$ is less critical for more slender girders, as the increase in stiffness is associated to a relatively appropriate decrease in capacity;

(iii) As for the IPE 330 parent section specimen, only small differences to Eurocode 3 curve *a* further confirms that the value of M_{cr} is the key parameter here. As M_{cr} was calculated accurately through the shell models, it can be shown of great importance for accurate design predictions, namely with respect to warping torsion contributions (see [1] for detailed results and analyses on these aspects);

(iv) Results are also shown to be relatively close to Eurocode 3 buckling curve *a* [34], which is the one relevant for the parent sections.

All these observations tend to suggest that resorting to the section with holes for the calculation of the relative slenderness λ_{LT} though $M_{pl\,hole}$ is the one to refer, as previously mentioned.

4. Development of F.E. models and validation

4.1 Modelling assumptions

Numerical modelling of the different test configurations was achieved by means of software FINELg, continuously developed at the University of Liège and Greisch Engineering Office since 1970 [35]. G.M.N.I.A. (Geometrical Material Non-linear Imperfection Analyses) calculations involving quadrangular 4-nodes plate-shell finite elements with typical features (Corotational

Total Lagrangian formulation, Kirchhoff's theory for bending) were performed. Density tests on the shell meshes used here were preliminary performed in order to guarantee the suitability of the numerical modelling.

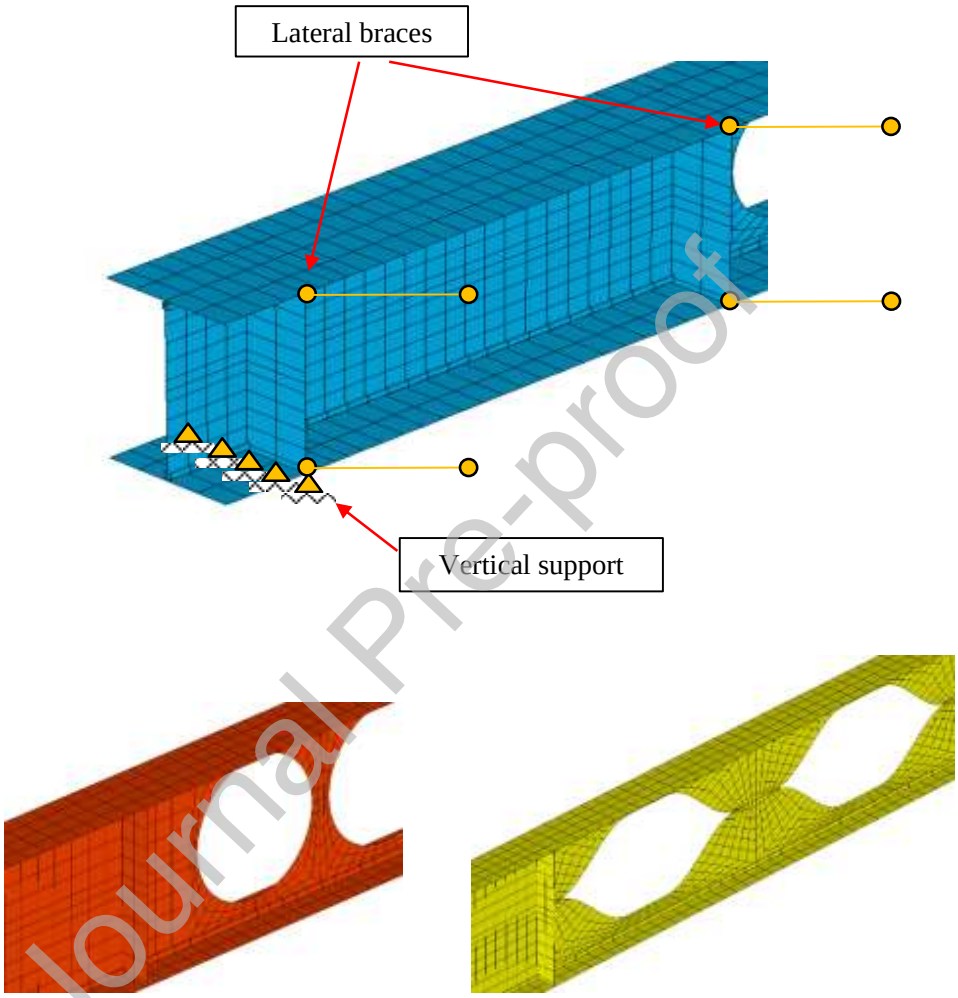

Fig. 18 – F.E. modelling of tests – a) Support conditions – b) Mesh pattern (left: IPE 330, right: Angelina).

Shell models of the experimental setup conditions were developed including all preliminary measured data, namely the geometry and dimensions of the girders, the measured thicknesses, σ-ε constitutive laws (multi-linear laws with a plastic plateau were adopted with corresponding values as in Table 1, see typical shape in Fig. 3) and recorded initial geometrical imperfections. Moreover, the numerical boundary and support conditions were derived so as to be as close as

possible to the experimental ones (see Fig. 18). As a particular point, residual stresses were not accounted for in the shell models; this was motivated by the fact that (i) the actual state of residual stresses in such girders is highly complex, since it results from a series of industrial processes having important effects on the distribution of residual stresses (base profile hot-rolling, flame cutting, final re-welding) and (ii) because it is of standard practice to sometimes locally apply important flame heating in the regions of the web that may lie outside the fabrication tolerances; these unpredictable operations definitely ruin the possibility to scientifically predict the state of residual stresses in such members.

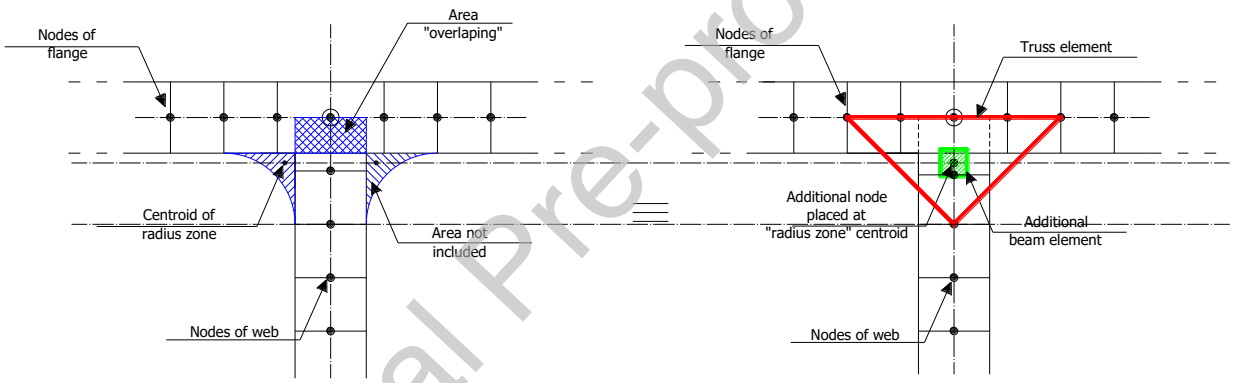

Fig. 19: F.E. treatment of web-to-flange junction.

Besides, F.E. modelling of the web-to-flange zone received a specific treatment. Within shell modelling, this region indeed suffers from (i) an overlap of material (see blue rectangle on Fig. 19, where some fibres are accounted for twice, as belonging both to an element of the web and to elements of the flange) and from (ii) the disregarding of flange radius areas (Fig. 19). In order to get closer to the real characteristics of such steel cross-sections, an additional node was placed within the web height, at the position of the centroid of the radius zone. This node also supported a supplementary beam element, oriented in the longitudinal direction and whose (square) cross-sectional area was equal to that of the radius zones minus the overlapped area. This extra beam element allowed to fix the above-mentioned two problems and led to nearly-

exact cross-sectional properties of the shell element in comparison to analytical ones[4]; this supplementary element was also provided the same constitutive law as the one of the plate elements. Moreover, three elastic truss elements forming a rigid triangle have been added in the web-flange area in order to keep this zone unaffected by an eventual extent of local buckling (Fig. 19): indeed, the presence of the flange radius keeps this area stiffer than the flat parts of the adjacent plates and helps reducing the proneness to local buckling. As a matter of fact, if any local buckling is likely to happen in one of the plates, it shall develop from the root of the fillets, not from the node joining web and flange, hence the need to stiffen this area, which was done through this truss system – further related details are also available in [36] and [37].

4.2 Assessment of numerical models against test data

Table 5 reports the results of the comparisons between the experimental and numerical results; as can be seen, a maximum of 8% difference in peak loads is obtained in the case of the IPE 330 parent section cellular girder. Fig. 13 to Fig. 16 further compare the numerical vs. experimental load-displacement behaviour of the specimens, and show a good agreement between the tests and the F.E. models. In addition, both the elastic bending stiffness of the system and post-peak behaviour were reasonably well captured by the numerical models, as the figures show. Fig. 17 also allows for comparisons in $\chi_{LT} - \lambda_{LT}$ axes, where λ_{LT} values for the F.E.A. plots are obviously equal to test ones, but slightly different χ_{LT} values from tests and F.E.A. results are visible.

[4] Complementary calculations allowed to validate this assertion and evidenced very close cross section properties between the F.E. model and its theoretical counterpart, except for what regards the Saint Venant's torsional constant I_t – the latter was proved to have a negligible influence on all configurations investigated herein.

Table 5: Comparison between tests and F.E. results (at peak load).

Specimen		P_{max} $[kN]$	M_{max} $[kNm]$	$\Delta_{vert.\ max}$ $[mm]$	$\Delta_{lat.\ max}$ $[mm]$	ψ_{max} $[rad]$
HEA 340	Test	1977.0	1087.4	75.1	15.3[2]	0.035
	F.E.M.	2071.9	1139.6	68.5	2.2	0
	Ratio	*0.95*	*0.95*	*1.10*	*6.95*	–
IPE 330	Test	176.9	172.0	62.3	24.5	0.075
	F.E.M.	191.6	186.4	65.1	26.8	0.108
	Ratio	*0.92*	*0.92*	*0.97*	*0.91*	*0.69*
Angelina	Test	235.1	258.6	59.4	6.35	0.015
	F.E.M.	226.9	249.5	56.2	13.4	0
	Ratio	*1.04*	*1.04*	*1.06*	*0.47*	–

Detailed analysis of the results in the case of the HEA 340 parent section suggests that the absence of residual stresses in the numerical model shall explain the fact that the experimental and F.E.-predicted load-displacement responses in Fig. 13a begin to slightly diverge beyond a load of about 1800 *kN*. Residual stresses indeed tend to deteriorate the member's stiffness prematurely, and this is clearly observed in Fig. 13a and Fig. 13b. Just as regular hot-rolled girders do, cellular beams bear compressive residual stresses at the flanges' tips. When combined with compressive stresses arising from bending, the residual stresses lead to early yielding in the tips, compared to situations where no residual stresses are present. Consequently, the fibres in the tips experience an important drop in stiffness, and the overall section suffers from a "premature" bending stiffness reduction (visible in Fig. 13a), ultimately leading to larger displacements. This explains the divergence observed between test data (where residual stresses are present) and F.E. data (no residual stresses) in a case where the member possesses a moderate L.T.B. slenderness ($\lambda_{LT} \approx 0.6$) where interactions between yielding and imperfections have the biggest impact.

Still, the numerical model is found in quite good agreement with the test results, in particular for initial stiffness and peak load prediction which is just 5% above the experimental one. As for

lateral displacements, since the response of the girder is seen to be inelastic yet rather close to a full plastic behaviour (see Fig. 17 and Table 4, χ_{LT} = 0.91), it is not surprising to observe sudden and rapidly increasing sway displacements when approaching a full yielding of the mid-span section, which arises close to peak load for the F.E. model but beginning from 1800 kN in the test, owing to compressive residual stresses at the flanges' tips [24].

In contrast, the IPE 330 parent section beam and the Angelina girder behave mostly elastically up to failure, characterizing an important influence of L.T.B. The observed gradual lateral drift is nicely captured by the F.E. models, as well as initial stiffness and post peak behaviour – note in particular the good correspondence for torsional twist in Fig. 16b. Numerical and test failure loads are in accordance within 8% for the IPE 330 parent section beam, and within 4% for the Angelina girder.

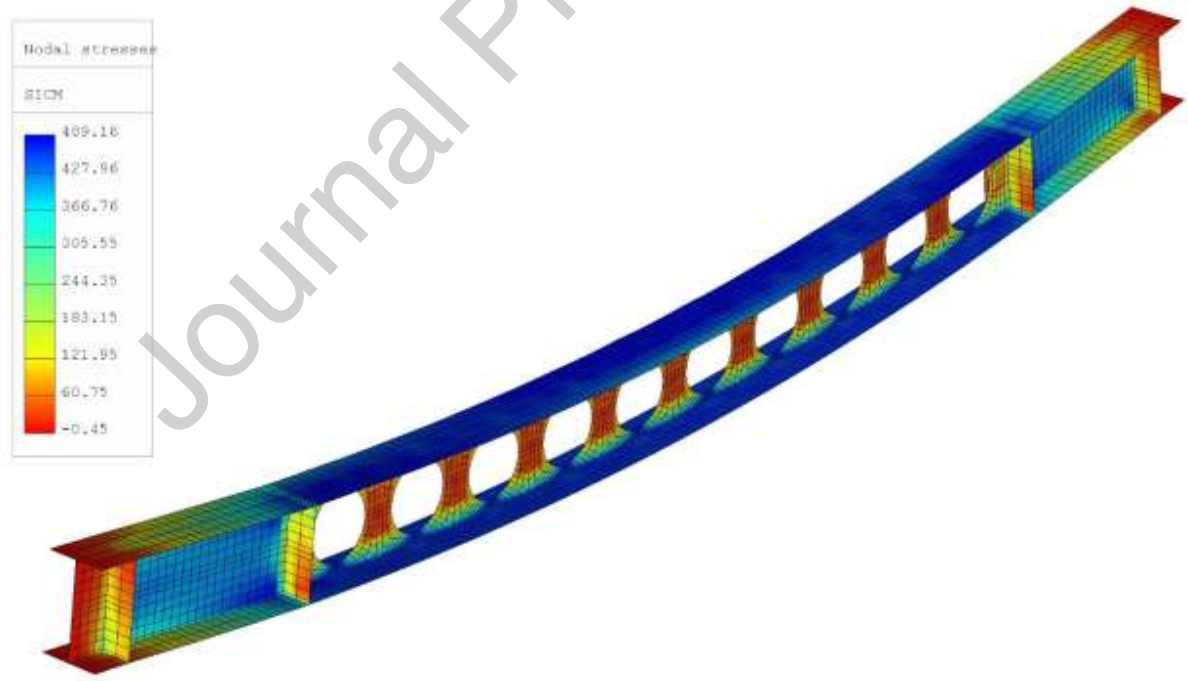

Journal Pre-proof

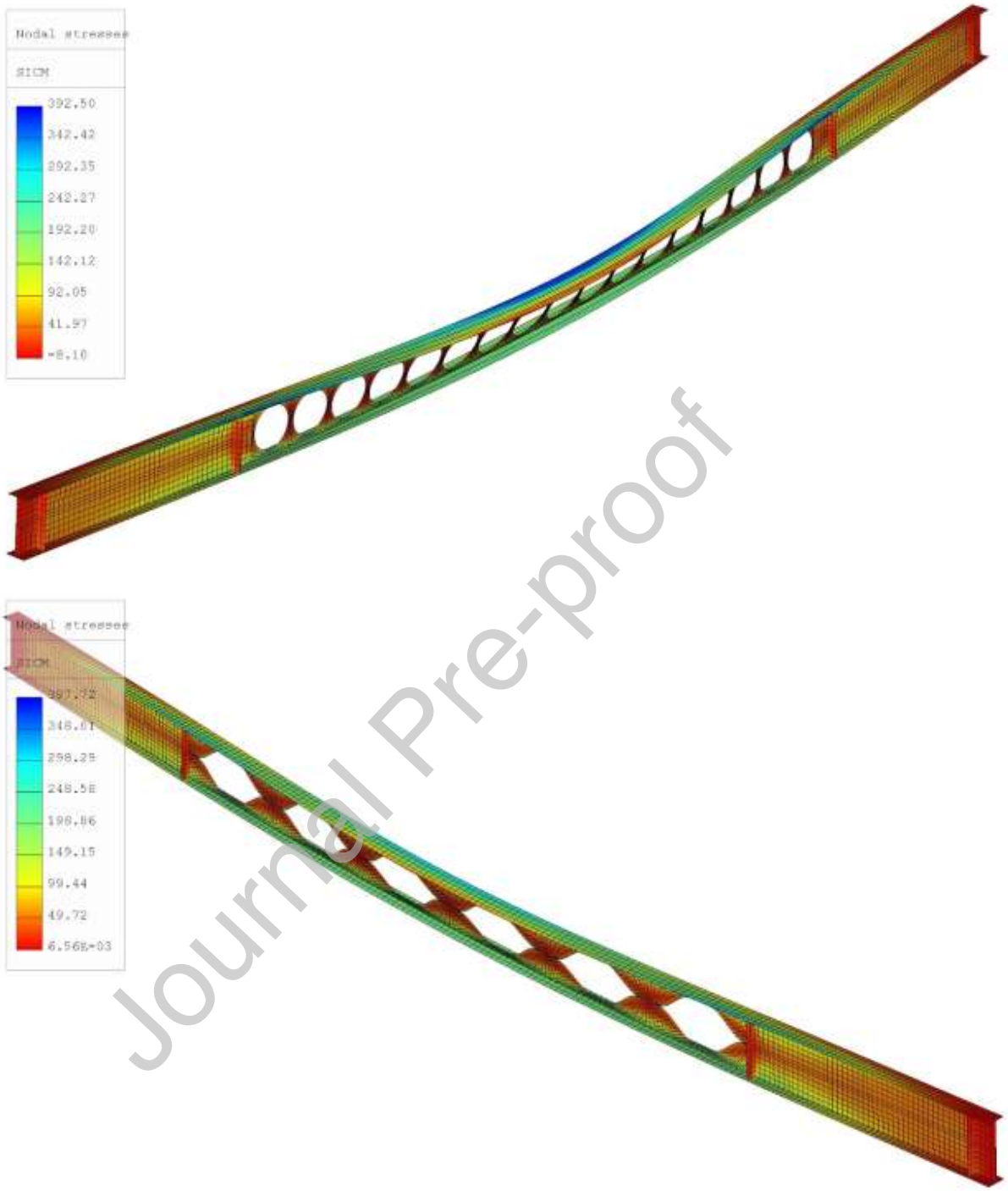

Fig. 20: F.E. (deformed) configuration and Von Mises stress distributions at peak loads – Upper: base profile: HEA 340 – Middle: base profile: IPE 330 – Lower: Angelina (amplification factor = 5 in all figures).

Eventually, Fig. 20 displays Von Mises stress distributions as well as deformed shapes at peak loads; the latter can be shown in quite good agreement with what was observed during testing

Journal Pre-proof

(e.g., Fig. 12). Combined with the numerical results reported previously, this further demonstrates that the shell models are able to provide reliable results (i.e., ultimate loads) and may safely be "substituted" to physical tests; they have been further used in extensive numerical studies.

5. Conclusions

The present paper investigated the lateral torsional buckling resistance of cellular steel beams, through experimental and numerical aspects. The results of three full-scale tests were first detailed; these consisted in 4-point bending tests, two on so-called "cellular beams" (from IPE 330 and HEA 340 parent sections) and another one on an Angelina girder (base profile: IPE 330). Spans were chosen from 7.5 m to 11.0 m with a maximized central segment under constant bending moment, so that lateral torsional buckling governed failure.

Careful preliminary measurements of dimensions and material laws were reported, as well as special efforts towards the measurement of initial geometric imperfections. The latter were determined through the combination of three purposely-developed optical systems, and, ultimately, a 3D representation of each girder could be provided, with a global accuracy of ± 0.3 mm.

The main tests showed typical lateral torsional buckling failure with the middle span sections experiencing simultaneous vertical and lateral deflections, combined with torsional twist. Yet, as a result of careful selections of spans and loading arrangement, the response of the girder varied from "inelastic L.T.B." with failure load close to the plastic capacity of the section to "elastic L.T.B.", characterized by sharp decreases in resistance immediately after the elastic part, at load levels quite below the plastic section capacity.

Detailed comparisons showed that for the tests encompassed here, (i) use of European Standards L.T.B. curve "*a*" shows adequate (this one is the curve relevant for the parent sections) despite high h / b ratios and that (ii) use of section properties accounting for the presence of the hole leads to more accurate resistance predictions. Results also evidence the increased key role of the critical bending moment M_{cr} for long beams – the latter are to be expected in practical applications.

All this information was implemented into shell models, built to simulate as closely as possible the behaviour observed in the tests; specificities in the numerical models such as the modelling of the web-to-flange area were also given. Detailed analysis of the results showed a quite good agreement between both experimental and numerical sources, both in terms of stiffness and of predicted peak loads, the maximum difference being only 8%. The F.E. models were consequently adopted for further numerical parametric studies, as detailed in the companion paper [1].

Acknowledgements

ArcelorMittal Commercial Sections is gratefully thanked for having provided the steel specimens used within the experimental investigations, as well as Prof. V. Barras, M Staub and colleagues, for their contributions to the measurement and numerical treatment of the initial geometrical imperfections.

References

[1] Boissonnade, N., Nseir, J., Somja, H. (2023). "Design of cellular steel beams subjected to lateral torsional buckling". *Submitted to Thin-Walled Structures.*

[2] Nethercot, D., Kerdal, D. (1982). "Lateral-torsional buckling of castellated beams". *The Structural Engineer, 60b, pp. 53–61.*

Journal Pre-proof

[3] Kerdal, D., Nethercot, D. (1984). "Failure Modes for Castellated Beams". *Journal of Constructional Steel Research, 4, pp. 295–315.*

[4] ECSC (2002). "Lateral torsional buckling in steel & composite beams", *project n° ECSC 7210-PR-183.*

[5] Radic, I., Markulak, D., Veravac, D. (2008). "Numerical simulation of lateral stability of castellated beams". *Proceedings of the 5th European Conference on Steel Structures, Eurosteel 2008, Graz, pp. 1593-1598, September 3-5.*

[6] El-Sawy, K, Sweedan, A., Martini, M. (2009). "Major-axis elastic buckling of axially loaded castellated steel columns". *Thin-Walled, Structures, 47, pp. 1295–1304.*

[7] Sweedan, A. (2011). "Elastic lateral stability of I-shaped cellular steel beams". *Journal of Constructional Steel Research, 67, pp 151–163.*

[8] Zirakian, T., Showkati, H. (2006). "Distortional buckling of castellated beams". *Journal of Constructional Steel Research, 62, pp. 863–871.*

[9] Lakusic, V. T., Dzeba, I., Androic, B. (2008). "The buckling curve for lateral-torsional buckling resistance of castellated beams". *Proceedings of the 5th European Conference on Steel Structures, Eurosteel 2008, Graz, pp. 1587-1592, September 3-5.*

[10] Ellobody, E. (2011). "Interaction of buckling modes in castellated steel beams". *Journal of Constructional Steel Research, Vo. 67 (814-825).* doi:10.1016/j.jcsr.2010.12.012.

[11] Verwij, J. (2010). "Cellular beam-columns in portal frame structures". *Master thesis, T.U. Delft.*

[12] Jian-zu Gu, Shanshan Cheng, "Shear effect on buckling of cellular columns subjected to axially compressed load", *Thin-Walled Structures 98 (2016) 416–420,* http://dx.doi.org/10.1016/j.tws.2015.10.019.

Journal Pre-proof

[13] Pattamad Panedpojaman, Worathep Sae-Long, Thaksin Thepchatri (2021), "Design of cellular beam-columns about the major axis", Engineering Structures 236, 112060, https://doi.org/10.1016/j.engstruct.2021.112060.

[14] Bitar, D., Martin, P.O., Galéa, Y., Demarco, T. (2006). "Poutres cellulaires acier et mixtes : partie 1 proposition d'un modèle pour la résistance des montants". *Construction Métallique n°1*.

[15] Martin, P.O., Galéa, Y., Bitar, D., Demarco, T. (2006). "Poutres cellulaires acier et mixtes : partie 2 proposition de nouveaux modèles analytiques de calcul de la fleche". *Construction Métallique n°2*.

[16] P.-O. Martin, M. Couchaux, O. Vassart, A. Bureau. "An analytical method for the resistance of cellular beams with sinusoidal openings", *Engineering Structures 143 (2017) 113–126, http://dx.doi.org/10.1016/j.engstruct.2017.03.048.*

[17] Sonck, D., Vanlaere, R., Van Impe, R. (2010). "Elastic buckling of cellular members loaded by an axial force". *Proceedings of the International Association for Shell and Spatial Structures (IASS) Symposium 2010, Shanghai*.

[18] Sonck, D., Van Impe, R. (2011). "Elastic Buckling of Cellular Members Loaded by an Eccentric Axial Force". *Proceedings of the 6th European Conference on Steel Structures, Eurosteel 2011, Budapest, August 31 - September 2*.

[19] Melissa Kerkhove, "Global buckling of eccentrically loaded cellular members", *Master of Science in Civil Engineering, U Ghent, 2015.*

[20] Pattamad Panedpojaman, Thaksin Thepchatri, Suchart Limkatanyu (2014), "Novel design equations for shear strength of local web-post buckling in cellular beams", Thin-Walled Structures, Vol. 76 (92-104), http://dx.doi.org/10.1016/j.tws.2013.11.007

Journal Pre-proof

[21] Rabee Shamass, Federico Guarracino (2020), "Numerical and analytical analyses of high-strength steel cellular beams: A discerning approach", Journal of Constructional Steel Research 166 105911, https://doi.org/10.1016/j.jcsr.2019.105911.

[22] Caroline Correa de Faria, Hermes Carvalho, Ricardo Hallal Fakury, Lucas Figueiredo Grilo (2021), "Lateral-torsional buckling resistance of cellular steel beams at room temperature and fire situation", Engineering Structures 237, 112046, https://doi.org/10.1016/j.engstruct.2021.112046.

[23] ECSC (2004). "Large Web Openings for Service Integration in Composite Floors", Project n°7210-PR-315.

[24] Sonck, D. (2014), "Global buckling of castellated and cellular steel beams and columns". PhD Thesis, Ghent University.

[25] Delphine Sonck, Jan Belis (2015), "Lateral–torsional buckling resistance of cellular beams", *Journal of Constructional Steel Research 105 (2015) 119–128, http://dx.doi.org/10.1016/j.jcsr.2014.11.003.*

[26] Pattamad Panedpojaman, Worathep Sae-Long, Tanan Chub-uppakarn. "Cellular beam design for resistance to inelastic lateral–torsional buckling", *Thin-Walled Structures 99(2016)182–194,* http://dx.doi.org/10.1016/j.tws.2015.08.026.

[27] Felipe Piana Vendramell Ferreira, Alexandre Rossi, Carlos Humberto Martins (2019), "Lateral-torsional buckling of cellular beams according to the possible updating of EC3", Journal of Constructional Steel Research 153 222–242, https://doi.org/10.1016/j.jcsr.2018.10.011.

[28] Sharifi, Y.; Tohidi, S., "Lateral-torsional buckling capacity assessment of web opening steel girders by artificial neural networks—Elastic investigation". Front. Struct. Civ. Eng. 2014, 8, 167–177.

[29] Miguel Abambres, Komal Rajana, Konstantinos Daniel Tsavdaridis, Tiago Pinto Ribeiro (2019), "Neural Network-Based Formula for the Buckling Load Prediction of I-Section Cellular Steel Beams", Computers 2019, 8(1), 2; https://doi.org/10.3390/computers8010002.

[30] Felipe Piana Vendramell Ferreira, Rabee Shamass b, Vireen Limbachiya, Konstantinos Daniel Tsavdaridis, Carlos Humberto Martins (2022), "Lateral–torsional buckling resistance prediction model for steel cellular beams generated by Artificial Neural Networks (ANN)", Thin-Walled Structures 170, 108592, https://doi.org/10.1016/j.tws.2021.108592.

[31] Mohamed El Amine Ben Seghier, Hermes Carvalho, Caroline Correa de Faria, José A.F.O. Correia, Ricardo Hallal Fakury (2023), "Numerical analysis and prediction of lateral- torsional buckling resistance of cellular steel beams using FEM and least square support vector machine optimized by metaheuristic algorithms", Alexandria Engineering Journal, Volume 67, Pages 489-502, https://doi.org/10.1016/j.aej.2022.12.062.

[32] Staub, M. (2011). « Combinaison de procédés topométriques pour le contrôle géométrique de poutres métalliques », MSc. Thesis, Yverdon-les-Bains : HEIG-VD.

[33] ACB+ (2022). ArcelorMittal Cellular Beams software ACB+ v4.02, Long Carbon Europe Research Centre.

[34] European Committee for Standardization (CEN) (2018). "PrEN 1993-1-1: Eurocode 3 – Design of Steel Structures – Part 1-1: General Rules and Rules for Buildings", Brussels.

[35] Non-linear finite element analysis program "FINELg" (2022), User's Manual, ArGEnCo Department, University of Liège, Greisch Info S.A., Liège, Belgium.

[36] Gérard, L., Li, L., Kettler, M. and Boissonnade, N. "Steel I-sections resistance under compression or bending by the Overall Interaction Concept". Journal of Constructional Steel Research. Vol. 182, pp. 106644, 2021. https://doi.org/10.1016/j.jcsr.2021.106644

Journal Pre-proof

[37] Li, L. and Boissonnade, N. “Local/global coupled instabilities of slender I-sections under compression”, Thin-Walled Structures, 172, pp. 108842, 2022. https://doi.org/10.1016/j.tws.2021.108842

We confirm that the manuscript has been read and approved by all named authors and that there are no other persons who satisfied the criteria for authorship but are not listed. We further confirm that the order of authors listed in the manuscript has been approved by all of us.

Declaration of interests

☐ The authors declare that they have no known competing financial interests or personal relationships that could have appeared to influence the work reported in this paper.

☒ The authors declare the following financial interests/personal relationships which may be considered as potential competing interests:

Nicolas Boissonnade reports equipment, drugs, or supplies was provided by ArcelorMittal.

Journal Pre-proof